MALS commissioning observations of PKS1830-211

(N. Gupta, P. Jagannathan)

March 24, 2020

1. Description of the target and observations

(For a quick summary see last section *Concluding remarks*)

The field centered at PKS1830-211 was observed on December 19, 2019 with MeerKAT-64 array. The target PKS1830-211 at z=2.507 is a well-known gravitationally lensed quasar. It has a flux density of 10.896 Jy at 1.4 GHz (cf. NVSS). This quasar sight line is remarkably unique: it has two HI 21-cm absorbers, one at z=0.190 and another at z=0.885 (Lovell+96; Chengalur+99). The z=0.885 absorber which corresponds to the lensing galaxy is particularly special. It exhibits numerous absorption lines corresponding to various molecular species (Wiklind+96; Muller+11). The extremely strong radio continuum and the presence of several absorption lines makes this sight line an appropriate target to test MeerKAT L- and UHF-bands.

For the observations, the total bandwidth of 856 MHz centered at 1283.9869 MHz was split into 32768 channels (frequency resolution = 26.123 kHz). The correlator dump time was 8 seconds and the data were acquired for all 4 polarization products, labelled XX, XY, YX and YY. These are first MALS commissioning observations using SKARAB correlator's 32K mode. Of the 64 antennas, 63 participated in the observation (m052 was unavailable). At the start of observation, we observed PKS1934-638 for 15 mins for flux density, delay and bandpass calibrations. The target source was observed for a total duration of 40 mins. Since PKS1830-211 is a bonafide calibrator for VLA at C- and D-arrays, there was no need to observe a gain calibrator separately.

The full dataset in measurement set format (1.5 TB) was staged at IDIA and then transferred to IUCAA over the internet. The processing was done on the VROOM cluster at IUCAA using the latest version of ARTIP based on CASA 5.6.1 (details at: https://mals.iucaa.in/releases).

2. Data Analysis: flagging and calibration

For this report we are interested only in stokes-I properties, so we generated a measurement set with only XX and YY polarization products and frequency channels 512 - 31230. This measurement set with 30720 frequency channels was processed using ARTIP-CAL as described below.

Since observatory-based level-0 flags may clip any strong spectral lines present in the data and remove short baselines both of which are of interest to MALS, we did not

consider these for our analysis. We also do not flag the antennas (m029v, m021v, m009v, 'm006v, m020v, m005v, m051v) suspected to be affected by SKARAB 32K artefacts.

We flagged the data only for NaNs and zeros, applied a very conservative RFI mask to eliminate the strongest RFI spikes seen in the data. These RFI spikes are present at all times even on the longest baselines. This initial mask is shown as shaded regions in the full 32K spectrum presented in Section 4.

We noticed that about 30 baselines (mostly <100m) on PKS1934-638 show unusual ripples across the L-band (also see Section 5). We flagged these on the primary calibrator. After predicting the model visibilities for the calibrator defined by "Stevens-Reynolds 2016" flux density scale ([I=13.993, Q=0, U=0, V=0] Jy @ 8.56e+08Hz), the pipeline performed initial calibration on a subset of frequency channels (19000~20000) to identify any non-working antennas or baselines. No additional flagging was needed at this stage.

Next, the pipeline proceeded to calibrate the entire band. First, strong RFI was flagged using Tfcrop. Then, flux density, delay and bandpass calibration were performed. After applying these calibrations but without any calibration-based flagging, the data on PKS1934-638 was further flagged for RFI using Rflag. After this the flux density, delay and bandpass calibrations were performed again. All the delays are in the range: (-0.4, 0.4) ns, and we did not notice any change in these before or after Rflag, however banpdpass solutions after Rflag are substantially improved.

After this the pipeline performed the gain calibration on PKS1830-211 and rescaled the calibration solutions. The flux density of PKS1830-211 at 1365.7 MHz is 11.1376 +/- 0.0129911. This matches with the NVSS flux density to within 2%.

After this all the calibrations were applied to the target source and the corrected visibilities were split into a separate measurement set which was then flagged for RFI using Tfcrop and Rflag. Note that 1410-1430 MHz range was excluded from the RFI flagging stages.

The calibrated data were then processed using ARTIP-CONT and ARTIP-CUBE to perform wideband continuum and spectral line imaging, respectively.

3. Wideband radio continuum image

The ARTIP-CONT first creates a dataset suitable for continuum imaging. At this step, the data were averaged in frequency per 32 channels (~0.8 MHz) and a more stringent RFI mask to completely exclude band edges and RFI-affected regions was applied. The frequency range considered for continuum imaging is shown as horizontal dashed lines

in Fig. 2. Additionally, the resultant frequency averaged 960 channels were regridded along the frequency axis to obtain a measurement set with 16 physically distinct spectral windows.

We created a widefield broad band 6k x 6k continuum image with a pixel size of 2 arcsec, spanning ~3.3 deg using tclean in CASA. The w-projection algorithm was used as the gridding algorithm in combination with Multi-scale Multi-term Multi-frequency synthesis for deconvolution, with nterms = 2 and four pixel scales to model the extended emission. Two rounds of phase-only self-calibration were carried out along with a final round of amplitude and phase self-calibration. Imaging masks were appropriately adjusted between major cycles during imaging and self-calibration.

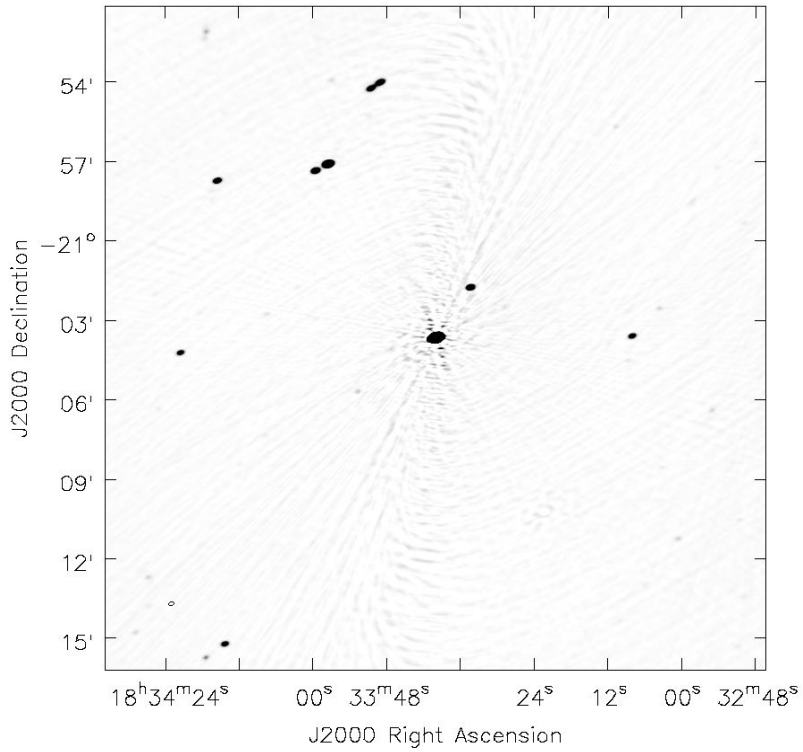

Fig.1 A portion of the larger 3.3deg image of PKS1830-211 (robust=0; no primary beam correction). The image sensitivity is 140 microJy and the contrast set to demonstrate the presence of the north-south imaging artefact that is present at that noise . The synthesized beam is: 12.9” x 8.1” (position angle = -76.3°).

The final image shown above has an imaging dynamic range of ~78500 made with robust weighting (robust=0) leading to a RMS sensitivity of 140μJy around the bright source and a RMS sensitivity of 40μJy away from the centre. The correlated noise artefact in the north-south direction around the bright central source, is saturated to be

visible. For this image this is the best achievable sensitivity in the absence of baseline-based or direction-dependent calibrations.

The central source PKS1830-211 is a known southern hemisphere calibrator whose continuum flux density was recovered to be 11.2446 +/- 0.0007 Jy at the reference frequency of 1.27 GHz. The in-band integrated spectral index is, alpha = 0.13. The source is compact and unresolved at L-Band VLA in both C and D configurations while being barely resolved in our MeerKAT image.

4. Full 32K spectrum of PKS1830-211

The ARTIP-CUBE, starts with splitting the calibrated visibilities along the frequency axis to create measurement sets that can be processed independently on the cluster nodes. For PKS1830-211, we split 30720 frequency channels into 15 spectral windows. The adjacent spectral windows have an overlap of 256 channels (~7 MHz). The unique frequency ranges covered by these measurement sets are marked as vertical dashed lines in the figure presented below. For easier referencing, we label these as SPW-0 to -14.

The measurement sets for these SPWs are then processed for continuum imaging with self-calibration and cube imaging. For continuum imaging, a continuum dataset is generated for each spectral window after averaging 32 channels and excluding RFI-affected frequency ranges. The self-calibration is initiated by predicting model visibilities based on the wideband continuum image obtained in the previous section. Here also two rounds of phase-only and one round of amplitude-and-phase self-calibration were performed.

The self-calibration solutions were then applied to the line dataset. The continuum subtraction was performed using UVSUB method using CLEAN components obtained in the continuum imaging step described in previous para. The continuum subtracted visibilities were then inverted to obtain the stokes-I spectral line cube.

The full spectral resolution L-band stokes-I spectrum after removing the residual continuum is shown in Fig. 2. We do not find any impact of the 64-channel periodic power dips and 32K bandpass artefacts in the final spectrum.

The residual continuum subtraction flux in each SPW is of the order of 0.5% and the shape is anti-correlated with respect to the spectrum of PKS1934-638 which peaks (turnover) at ~1220 MHz. This implies that the residual continuum for SPWs 2 and 3 also has a curvature, which requires a smooth polynomial of higher order (4-6) for correction. For SPWs, 1, 4, 8-11 and 14 a linear fit is sufficient. The SPW-0 falls where the L-band starts rolling off. The residual curvature in this case can also be corrected similar to SPWs 2 -3.

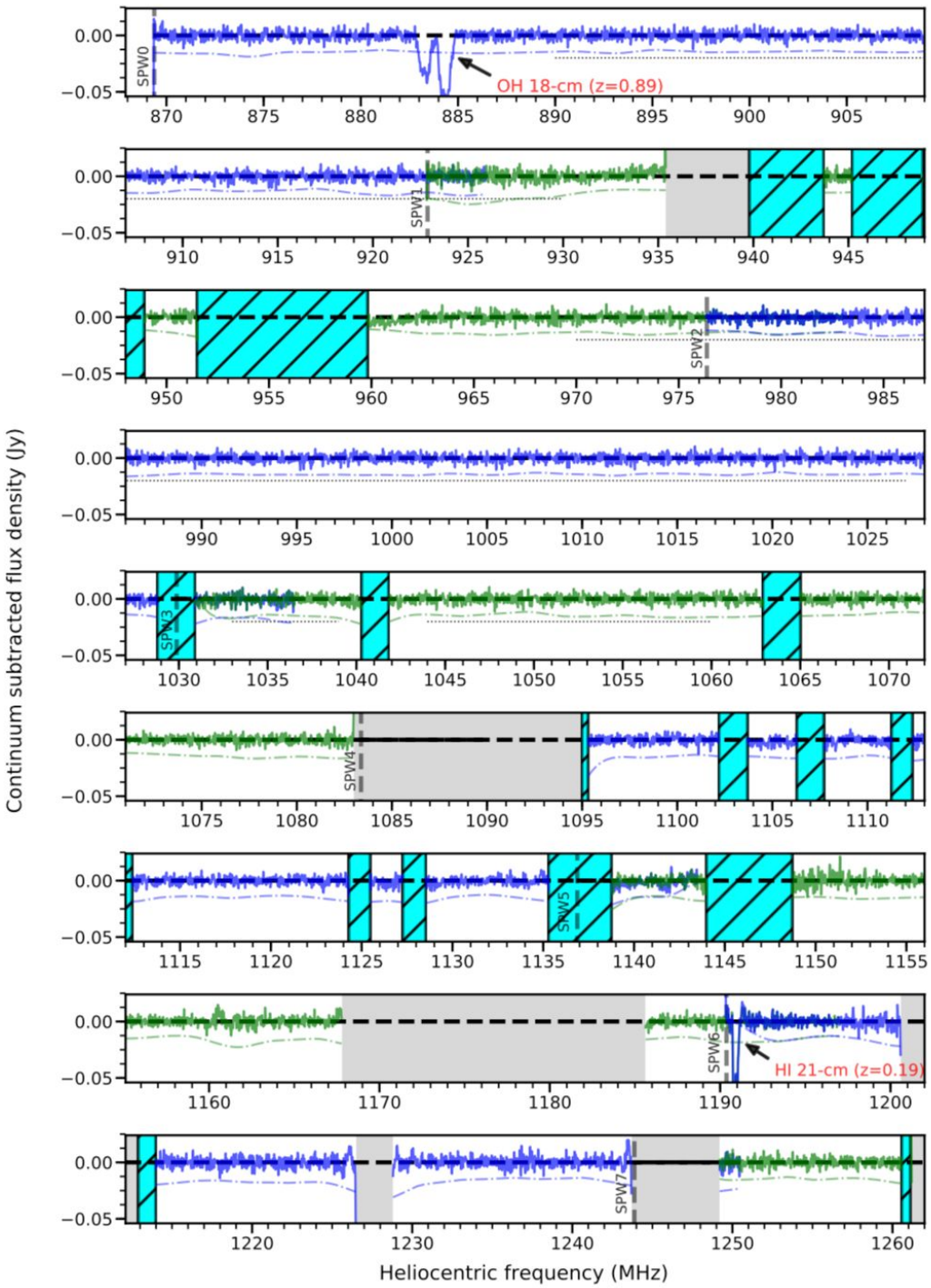

Fig. 2 L-band spectrum of PKS1830-211. Shaded region corresponds to the initial RFI mask described in Section 2. Hatched regions (corresponding to RFI spikes) were rejected after CUBE-imaging. Vertical dashed lines mark edges of SPW-0 to SPW-14 used to parallelize ARTIP-CUBE processing. The spectra from adjacent SPWs are plotted alternately in blue and green. The adjacent SPWs overlap by ~7 MHz. The Galactic HI 21-cm line and HI/OH absorption towards PKS1830-211 are labelled. Dashed-dotted line is the error spectrum (5σ).

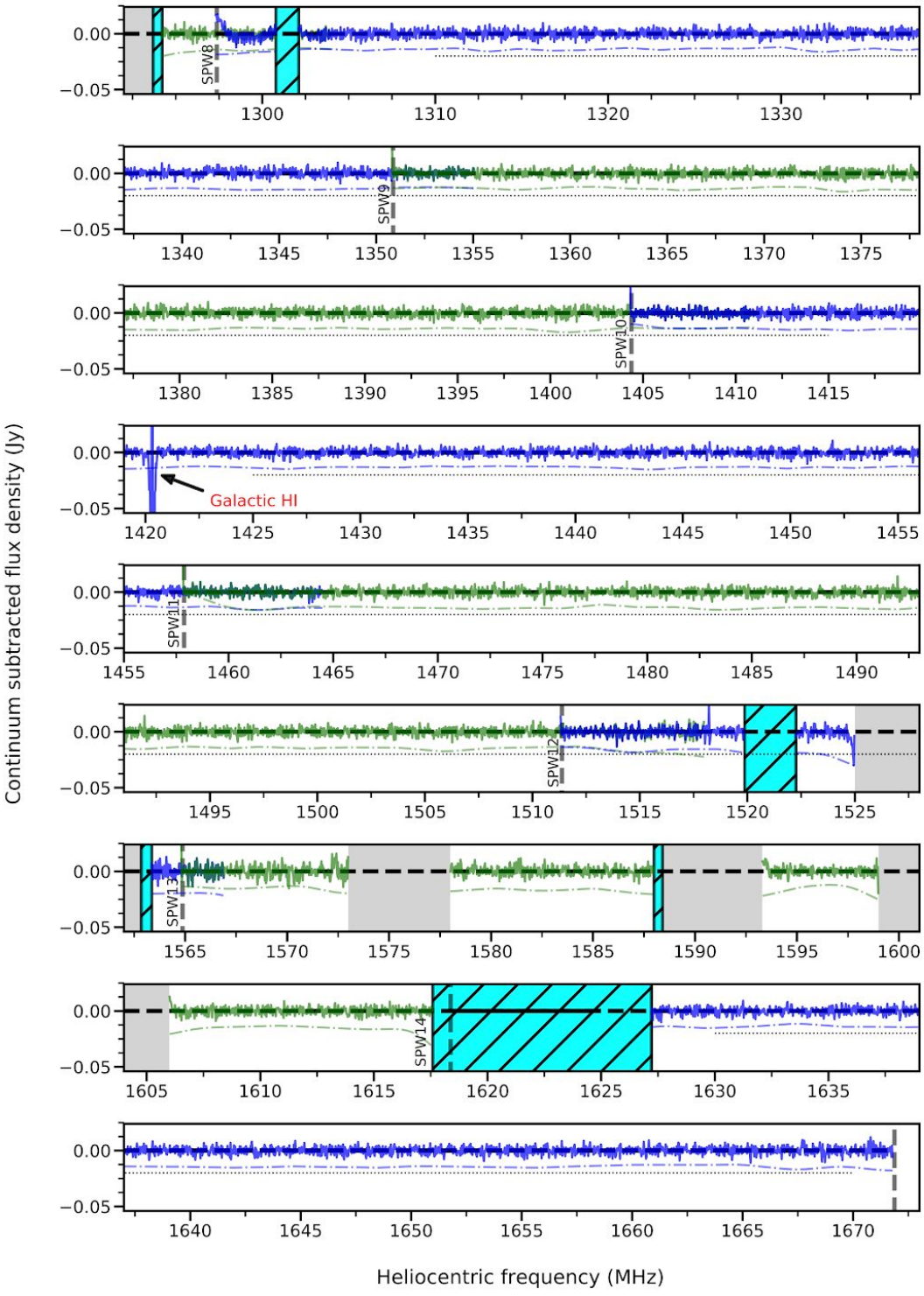

Fig. 2 Continued

To summarize, SPWs 0-4, 8-11 and 14 have extremely high spectral line fidelity. The spectral rms of 2.9 mJy/beam (Robust=0) in SPW 9 corresponds to a 3-sigma optical depth sensitivity of 0.0007 (i.e. sensitive to $6x10^{17}$ cm^{-2} for 100K gas). Most importantly there is excellent phase coherence till the extreme edge of the L-band (z~0.6 for HI 21-cm line) --> this is demonstrated by the detection of OH 18-cm main lines from the z=0.885 absorber.

The SPWs 5-7, 12 and 13 are affected by broadband RFI and have poor fidelity. But the detection of HI 21-cm line (z=0.19; at ~1190 MHz) with properties as expected from published absorption profiles demonstrates that useful spectral line science is possible in this frequency range as well. It is possible to quantify the fidelity and completeness of spectral lines that can be detected in this region -- but that discussion is beyond the scope of this report.

Finally, we note that the spectral rms measured towards PKS1830-211 shows only a minor improvement between Robust=0 (presented here) to Robust=2 (Natural weighting). Further, for 40 mins on target, at 1375 MHz we expect spectral rms of 0.7 mJy/b. But in SPW-9, for Robust=2 the measured rms is 2.7 mJy/b which is a factor 4 higher than the theoretical value.

For 15 mins on PKS1934-638, the signal-to-noise ratio (SNR) achieved in bandpass calibration should be adequate for 25 mins on PKS1830-211. To test whether the SNR in bandpass calibration is the limiting factor in our analysis, we also performed CUBE-imaging considering only t_int = 15 and 25 mins of data rather than the full 40 mins. In both the cases the spectral rms was found to be larger by sqrt(40/t_int) as expected. Therefore, it is unclear at this stage whether the factor 4 higher rms in the spectrum is due to dynamic range limitation (target source is ~11 Jy) or something else.

5. Open issues (under investigation)

Short baselines in the data (baseline length < 100m) show frequency dependent ripples that can't be removed by bandpass calibration. This is of concern in particular for spectral line observations and is present in the 32K channel mode. The magnitude of the effect seems to be independent of the baseline length as can be seen in the sample baseline plots shown below in Fig 3 of four baselines under a 100m in baseline length. The plots show the amplitude of the RR and LL visibilities (two colors) plotted as a function of the channels (frequency). Note that the lower end of the band (<16K channels) has significant rippling as against the higher end of the band. The frequency dependence of the ripple is stronger at the lower end of the band suggesting an inverse frequency scaling (proportional to wavelength). We are investigating the issue further in terms of its impact on our spectral data reduction and the effect of the exclusion of these

short baselines in our spectral line data reduction. These ripples may impact high-DR continuum imaging science.

We have shown a dynamic range limited continuum image of PKS1830-211 where the central source presents a north-south artefact at the sensitivity limit. We suspect that these errors are due to residual baseline-dependent amplitude and phase errors and are being explored in greater detail.

While the source that we have imaged as a test target has a flux density of ~11Jy and is not representative of a MALS source which is typically 0.5Jy in flux density. With that in mind we are evaluating the effect of the open issues on our spectral and continuum imaging pipelines, while trying to derive effective strategies to solve or mitigate them.

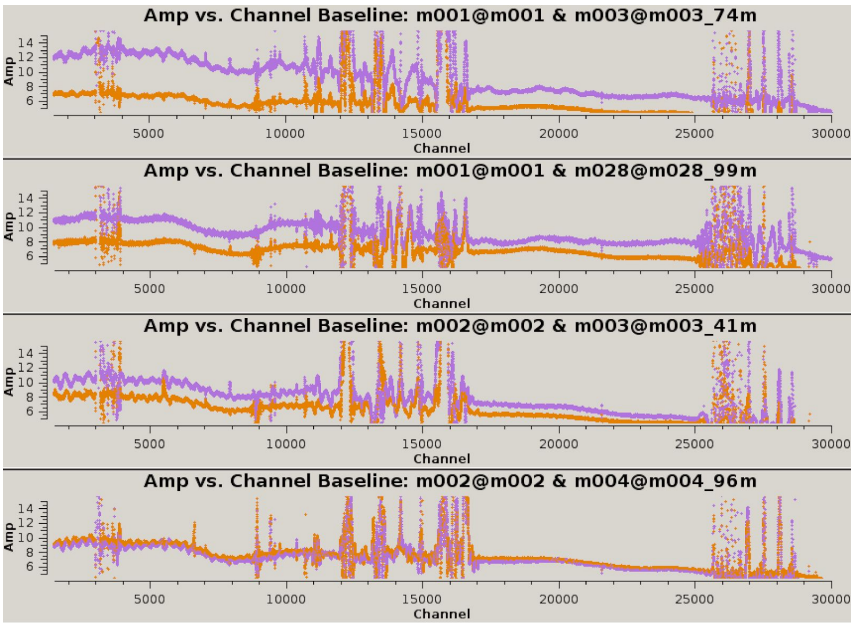

Fig 3. The time averaged visibility plot (2mins) showing the visibility amplitude as a function of channel (frequency) for the bandpass calibrator for 32K data with baseline lengths shorter than 100m. The rippling is more prominent at the lower half of the band.

6. Concluding remarks

The field centered at PKS1830-211 (10.86 Jy in NVSS) was observed on December 19, 2019 with MeerKAT-64 array. These are the first MALS commissioning observations using 32K mode of the SKARAB correlator. The data were processed using ARTIP on the VROOM cluster at IUCAA. The radio continuum properties of the source are consistent with the published results. The wideband radio continuum image has a dynamic range of ~78500. We detect known HI 21-cm (z=0.190) and OH 18-cm

(z=0.885) absorption lines towards the sight line. The data exhibit excellent spectral line fidelity across most of the L-band (optical depth sensitivity ~ 0.0007) and phase coherence up to the extreme edge of the band. The continuum subtraction is accurate up to 0.5%. However, the spectral rms is a factor of 4 higher than the theoretically expected value and needs to be investigated through observations of typical/ additional MALS fields.